ACS EARTH AND SPACE CHEMISTRY

http://pubs.acs.org/journal/aesccq

Article

# Observationally Constrained Modeling of the Reactive Uptake of Isoprene-Derived Epoxydiols under Elevated Relative Humidity and Varying Acidity of Seed Aerosol Conditions

Jie Zhang, Manish Shrivastava,* Alla Zelenyuk, Rahul A. Zaveri, Jason D. Surratt, Matthieu Riva, David Bell, and Marianne Glasius

Cite This: https://doi.org/10.1021/acsearthspacechem.2c00358

Read Online

ACCESS | Metrics & More | Article Recommendations | Supporting Information

**ABSTRACT:** Isoprene is the nonmethane volatile organic compound (VOC) emitted in the largest amounts to the atmosphere, and it is a significant source of secondary organic aerosol (SOA) mass. The uptake of isoprene oxidation products followed by multiphase chemistry in fine particles is the key pathway to form isoprene epoxydiol-derived SOA (IEPOX-SOA). However, many parameters that relate to the diffusion and reaction of IEPOX in the particle phase remain uncertain since reaction kinetics previously measured in bulk aqueous-phase solutions might be different from atmospheric aerosols. Here, we use simultaneous environmental chamber measurements of multiple parameters governing IEPOX-SOA formation at timescales of ∼hours: particle size distribution, composition, and volatility of IEPOX-SOA to constrain the key parameters governing IEPOX-SOA formation under humid (i.e., 50% relative humidity, RH) and varying seed aerosol acidity conditions. Reducing the 2-methyltetrol (tetrol) reaction rate constants by a factor of 4 brings the model predictions in agreement with the IEPOX-SOA measurements with acidified ammonium bisulfate seed aerosols. For less acidic ammonium sulfate aerosols, we find that both the organosulfate (OS) and tetrol reaction rate constants need to be reduced to bring model predictions closer to chamber observations. Using the measured nonvolatile content of IEPOX-SOA, we constrain the oligomerization timescale of tetrols. We find that the oligomerization timescale is 4 h with acidified seed aerosols, but a much longer timescale of 24 h is needed for nonacidified aerosols, indicating that the aerosol acidity greatly affects the oligomerization rate of tetrols. We show that the actual kinetics of IEPOX-SOA formation rate on aerosols consisting of both ammonium bisulfate and ammonium sulfate is a factor of 4−5 slower under 50−60% RH conditions compared to their application in previous models, which were mostly based on bulk aqueous solution measurements.

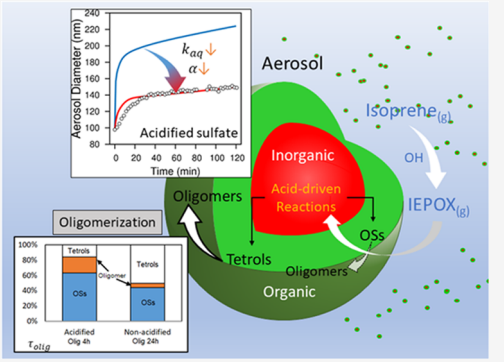


**KEYWORDS:** *IEPOX-SOA, reactive uptake, acid-driven reactions, tetrol oligomerization, elevated relative humidity*



## INTRODUCTION

Isoprene (2-methyl-1,3-butadiene, $C_5H_8$) is the largest emitted nonmethane biogenic volatile organic compound (VOC) in the atmosphere, with estimated global annual emissions of 500−750 Tg.[1] It can be readily oxidized by hydroxyl radical (OH),[2−4] ozone ($O_3$),[5,6] and nitrate radical ($NO_3$)[7−9] to generate semivolatile and low-volatile products that can condense on preexisting atmospheric particles to form secondary organic aerosol (SOA). Consequently, isoprene is a significant source of the global SOA budget.[10,11] The rapid reaction between isoprene and OH radical ($k$ = 9.7 × $10^{-11}$ $cm^3$ $molecule^{-1}$ $s^{-1}$) makes it the major pathway to form isoprene SOA in the atmosphere.[12,13] The branching ratio of initial products (i.e., peroxy radicals, $RO_2$) of isoprene + OH reaction is governed by the concentration of nitrogen oxides ($NO_x$ = NO + $NO_2$) and determines the subsequent SOA formation pathways.[14]

Under low-$NO_x$ conditions, isoprene hydroxyhydroperoxides (ISOPOOH) are formed with large yields (>70%) from the photooxidation (OH-initiated oxidation) of isoprene.[15,16] Subsequent OH reaction of ISOPOOH produces isomeric isoprene-derived epoxydiols (IEPOX) with yields exceeding 75%.[15] IEPOX isomers are recognized as important reactive intermediates in the formation of isoprene SOA.[17] The irreversible uptake of gas-phase IEPOX into acidic aerosol water is expected to generate isoprene SOA, including known semivolatile products 2-methyltetrols (2-methylthreitol and 2-methylerythritol, hereafter tetrols), and low-volatile organo-

Received: November 23, 2022
Revised: March 17, 2023
Accepted: March 17, 2023

sulfates (OSs) such as the methyltetrol sulfate (hereafter tetrol sulfate) monomers as well as oligomeric species of both tetrols and tetrol sulfates.[17−22] Among these products, tetrols[23,24] and tetrol sulfates[19,25] have been identified as organic tracers for isoprene-derived SOA under low-$NO_x$ conditions, which are measured in the ambient air and used to quantify the contributions from isoprene[26−30] to the total SOA. Accurately modeling tracer compounds along with other SOA species is useful to establish the links between organic tracers and source-specific SOA by avoiding biases due to different conditions between chamber experiments and the ambient environment.[31−33] Thus, modeling explicit IEPOX-derived SOA (IEPOX-SOA) components is critical to quantify the isoprene SOA in the ambient air based on field measurements of organic tracers.

The acid-driven multiphase chemistry mechanism was implemented in multiple regional chemical transport models (CTMs) to simulate IEPOX-SOA, and the results were compared with the field measurements and aircraft observations.[34−38] However, the chemical kinetics of IEPOX-SOA formation in aerosols is based on measurements in bulk solutions,[39] which may not apply to atmospheric aerosols. In addition, short timescale (∼seconds) flow tube experiments were used in previous studies to understand the uptake of gases,[40] but these flow tube experiments have limited utility in understanding the growth of particles during IEPOX-SOA formation, especially at longer atmospherically relevant times ∼hours.

Previous modeling studies have shown that IEPOX-SOA could contribute to approximately 10% of total SOA during the summertime in the eastern US with high isoprene emissions.[37] In most current models, the reduced version of Gas-Aerosol Model for Mechanism Analysis (simpleGAMMA)[41] box model was integrated to describe the uptake of gas-phase IEPOX and followed by acid-driven aqueous-phase reactions to produce SOA using the reaction rate constants and other parameters reported by Budisulistiorini et al.[38] However, Zhang et al.'s studies revealed the self-limiting effects of IEPOX-SOA formation due to aerosol-phase state and viscosity.[18,42] Considering the diffusion limitations by viscous SOA coatings,[43] Shrivastava et al.[36] implemented the IEPOX reactive uptake mechanisms and viscosity effects[44] into the Weather, Research and Forecasting model with Chemistry (WRF-Chem) to simulate IEPOX-SOA components over the Amazon Rainforest and investigated the land surface-aerosol−cloud interactions. They found that upper tropospheric IEPOX-SOA formation was governed by additional surface chemistry processes resulting in emissions of semivolatile 2-methyltetrol gases and their transport by deep convection to high altitudes.

IEPOX reactive uptake parameters and diffusion limitations with SOA coatings were evaluated by Octaviani et al.[45] using an extended resistor-based box model to simulate the chamber experiments with acidified sulfate aerosols under dry conditions (relative humidity (RH) <5%). The model of Octaviani et al. successfully captured the measured particle size evolution, chemical composition, density, and volatility. However, the IEPOX-SOA model has not been evaluated for experiments under higher atmospherically relevant RH conditions.

In this study, we applied the integrated IEPOX-SOA box model in Octaviani et al.[45] to investigate the kinetic processes governing the evolution of particle size distribution and chemical composition with IEPOX reactive uptake onto acidified and nonacidified ammonium sulfate seed aerosols under elevated-RH (50−60% RH) conditions.[43] Compared to those used in Octaviani et al.,[45] the IEPOX reactive uptake parameters (i.e., reaction rate constants, accommodation coefficient, and oligomerization time) were evaluated and constrained by the chamber-measured particle size distribution, aerosol number mean diameter, total suspended aerosol volume concentrations, and final SOA products' volatility and compositions. This work focuses on an aerosol system with sulfate seed aerosols of varying acidity under RH 50−60%.

## METHODS

**Chamber Experiments.** The chamber experimental study described by Riva et al.[43] provides the initial conditions for box modeling with gas-phase IEPOX concentration and size distribution of seed particles. The schematic of the chamber employed is shown in the Supporting Information of Octaviani et al.[45] Acidified sulfate seed aerosols (ammonium bisulfate, ABS) were generated by nebulizing aqueous solutions of 0.06 M $(NH_4)_2SO_4$ (aq) + 0.06 M $H_2SO_4$ (aq), while nonacidified sulfate seed aerosols (ammonium sulfate, AS) were generated by nebulizing aqueous solutions of 0.06 M $(NH_4)_2SO_4$ (aq) only. The experiments were conducted in a 1 $m^3$ Teflon chamber under elevated-RH conditions (58% RH for ABS and 51% RH for AS) at room temperature (24 ± 2 °C) and standard atmospheric pressure (1 atm). The seed particles were introduced into the Teflon chamber prior to IEPOX injection. Then, 2.5 mg of *trans*-$\beta$-IEPOX, which is the prevalent IEPOX isomer,[16] was injected into the chamber mixed with seed aerosols by passing high-purity $N_2$ gas at 2 L $min^{-1}$ through a heated manifold (60−70 °C) for 30 min, which resulted in the mixing ratio of 500 ppb in the chamber. The synthetic procedures for *trans*-$\beta$-IEPOX were described in the previous study.[46]

During the IEPOX reactive uptake onto seed aerosols, the size distributions of particle number and volume concentrations were periodically measured by a scanning mobility particle sizer (SMPS, TSI, Inc., model 3936), which consists of a differential mobility analyzer (DMA) and a condensation particle counter (CPC). Single-particle mass spectrometer (miniSPLAT)[47] was used to periodically characterize the size, density, shape, and mass spectra of individual particles in the chamber at a time resolution of several minutes. At the end of each experiment, the aerosols were collected on Teflon membrane filters (47 mm diameter, 1.0 $\mu$m pore size) at a low rate of ∼10 L $min^{-1}$ for 70−80 min, and the samples were analyzed offline to quantify IEPOX-SOA chemical composition using reversed-phase liquid chromatography/electrospray ionization, high-resolution quadrupole time-of-flight mass spectrometry (RPLC/ESI-HR-QTOFMS), and gas chromatography/electron ionization-mass spectrometry (GC/EI-MS) analysis. As described previously, a mixture of 2-methyltetrol sulfate esters (tetrol sulfates), 2-methyltetrols (tetrols), and *cis*- and *trans*-3-methyltetrahydrofuran-3,4-diols (3-MeTHF-3,4-diols) was synthesized in-house and used to quantify the IEPOX-SOA tracers.[43]

**IEPOX Gas Reactive Uptake.** The IEPOX reactive uptake onto sulfate seed aerosols is described by first-order reaction kinetics with the uptake coefficient $\gamma_{IEPOX}$ and particle surface area $A_p$ ($cm^2$ $cm^{-3}$), as eq 1

$$\frac{d[IEPOX_g]}{dt} = -\frac{\gamma_{IEPOX}}{4} A_p \langle c \rangle [IEPOX_g] \quad (1)$$


https://doi.org/10.1021/acsearthspacechem.2c00358
ACS Earth Space Chem. XXXX, XXX, XXX−XXX

**Table 1. Third-Order Reaction Rate Constants and Accommodation Coefficients Used in This Study**

| | | aqueous-phase reaction rate constants | | | | |
|---|---|---|---|---|---|---|
| | products | tetrols | | | OSs | |
| | nucleophile | water | | | sulfate | |
| | acids | $k_{H^+,j}$ ($M^{-2}$ $s^{-1}$) | $k_{HSO_4^-,j}$ ($M^{-2}$ $s^{-1}$) | $k_{NH_4^+,j}$ ($M^{-2}$ $s^{-1}$) | $k_{H^+,j}$ ($M^{-2}$ $s^{-1}$) | $\alpha$ |
| ABS[d] | *Base* | $9.00 \times 10^{-4}$ [a] | $1.31 \times 10^{-5}$ [a] | $3.10 \times 10^{-7}$ [b] | $1.27 \times 10^{-3}$ [c] | 0.02 |
| | *LowRxn* | $2.25 \times 10^{-4}$ | $2.62 \times 10^{-6}$ | $6.20 \times 10^{-8}$ | $1.27 \times 10^{-3}$ | 0.02 |
| | *LowAccom* | $2.25 \times 10^{-4}$ | $2.62 \times 10^{-6}$ | $6.20 \times 10^{-8}$ | $1.27 \times 10^{-3}$ | 0.001 |
| AS[e] | *Base* | $9.00 \times 10^{-4}$ | $1.31 \times 10^{-5}$ | $3.10 \times 10^{-7}$ | $1.27 \times 10^{-3}$ | 0.02 |
| | *LowRxn* | $1.80 \times 10^{-4}$ | $2.62 \times 10^{-6}$ | $6.20 \times 10^{-8}$ | $1.91 \times 10^{-4}$ | 0.02 |
| | *LowAccom* | $1.80 \times 10^{-4}$ | $2.62 \times 10^{-6}$ | $6.20 \times 10^{-8}$ | $1.91 \times 10^{-4}$ | 0.001 |

[a]Eddingsaas et al.[39] [b]Nguyen et al.[51] [c]Riedel et al.[52] [d]Tetrol oligomerization timescale for ABS is 4 h in all three cases. [e]Tetrol oligomerization timescale for AS is 24 h in all three cases.

where $[IEPOX_g]$ is the gas-phase IEPOX concentration (mol $m^{-3}$) and $\langle c \rangle$ is the mean molecular velocity (cm $s^{-1}$). The $\gamma_{IEPOX}$ is calculated based on a resistor-based model accounting for gas-phase diffusion, mass accommodation, and bulk-phase processes (dissolution, diffusion, and chemical reactions), as the three terms in order on the right-hand side of eq 2 described in Anttila et al.[48]

$$\frac{1}{\gamma_{IEPOX}} = \frac{\langle c \rangle r_p}{4D_g} + \frac{1}{\alpha} + \frac{\langle c \rangle r_p}{4RTH_{org}D_{org}(q_{org}F - 1)} \quad (2)$$

where $D_g$ is the gas-phase diffusion coefficient ($cm^2$ $s^{-1}$), which is estimated using $D_g = 1.9(MW)^{-2/3}$ with molecular weight (MW) of IEPOX (118 g $mol^{-1}$); $r_p$ is the radius of particle (cm), which contains the inorganic aqueous core and organic coating thickness; $\alpha$ is the mass accommodation coefficient of IEPOX; $R$ is the ideal gas constant (0.082 L atm $K^{-1}$ $mol^{-1}$); $T$ is the temperature (K); $q_{org}$ is a diffuso-reactive parameter describing the competition between diffusion and reaction within the organic coating; and $H_{org}$ and $D_{org}$ are Henry's law constant and diffusion coefficient of reactants in the organic coating, respectively. The $H_{org}D_{org}$ value was determined based on SOA viscosity measurements from a flow tube reactor conducted under RH of 40−99%.[42] $H_{org}$ was set to $2.0 \times 10^6$ M $atm^{-1}$ as used in Zhang et al.[42] The function $F$ represents a composite term for the processes involved in the reactive uptake at the interface between two bulk phases and can be calculated following eqs 3−6 in Octaviani et al.[45]

**Aqueous-Phase Acid-Driven Reaction Rate Constant.** The IEPOX-SOA formation can be described by pseudo-first-order acid-driven reactions in the aerosol water, and rate constant ($k_{aq}$, $s^{-1}$) is calculated assuming protonation of IEPOX and nucleophilic addition, as eq 3 described by Eddingsaas et al.[39]

$$k_{aq} = \sum_{i}^{N_{acid}} \sum_{j}^{N_{nuc}} k_{i,j}[acid_i][nuc_j] \quad (3)$$

where $N_{acid}$ and $N_{nuc}$ are the number of acids ($H^+$, $NH_4^+$, and $HSO_4^-$) and nucleophiles ($H_2O$ and $SO_4^{2-}$), respectively, and $[acid_i]$ and $[nuc_j]$ are the molar concentration of acids and nucleophiles (M), respectively. During the calculation, the $H^+$ activity ($a_{H^+}$) represents the molar concentration of $H^+$, which is adjusted by multiplying the $H^+$ activity coefficient based on E-AIM model.[49,50] Only the aerosol water content associated with the inorganic phase (M of aerosols) is used as nucleophile $H_2O$. $k_{i,j}$ is third-order reaction rate constants ($M^2$ $s^{-1}$). Their values are derived from previous kinetic studies[39,51,52] and summarized in Table 1 (base case), which were first compiled in Budisulistiorini et al.'s work[38] and applied in most current modeling studies.[36,37,44,45] In this study, these reaction rate constants were reassessed and constrained by the chamber-measured particle size evolution and SOA product composition (see Table 1, *LowRxn* case). The two major SOA products formed through the aqueous-phase reactions are tetrols and IEPOX-organosulfates (i.e., methyltetrol sulfates or OSs).[22] The molar fraction ($\beta$) of OSs in the total IEPOX-SOA was determined based on the relative contribution of the OSs formation rate to the effective first-order reaction rate constant ($k_{aq}$).

**IEPOX-SOA Formation Scheme.** Figure 1 illustrates the process of IEPOX multiphase reactive uptake onto the phase-separated aerosols, gas-particle-phase partitioning of tetrols, and their oligomerization process. It is well accepted that OS products have low volatility based on the measurements of evaporation kinetics of OS standards,[21,22] and they are treated as nonvolatile products in our model. Thus, the oligomerization process of OSs is not included in the present study, even though they have been previously demonstrated to participate in oligomerization within laboratory-generated and ambient aerosols.[17,20,43,53,54] However, the saturation mass concentration ($C^*$) for tetrols was estimated to be within a range of 5−15 $\mu g$ $m^{-3}$ reported by D'Ambro et al.,[22] and the average value of 10 $\mu g$ $m^{-3}$ is used in the model. Thus, the tetrols are treated as semivolatile and can be kinetically partitioned into the gas phase. The diffusion-limited partitioning of tetrols is

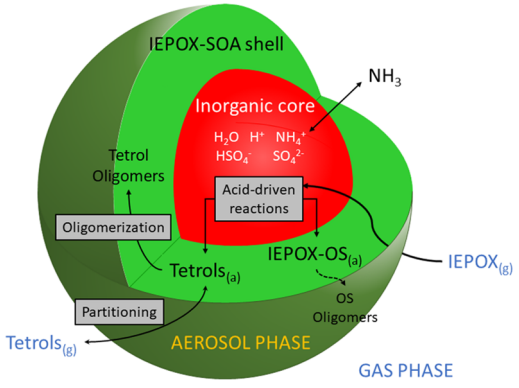


**Figure 1.** Schematic of IEPOX-SOA formation through multiphase reactive uptake of IEPOX and tetrols partitioning and oligomerization processes.


https://doi.org/10.1021/acsearthspacechem.2c00358
ACS Earth Space Chem. XXXX, XXX, XXX−XXX

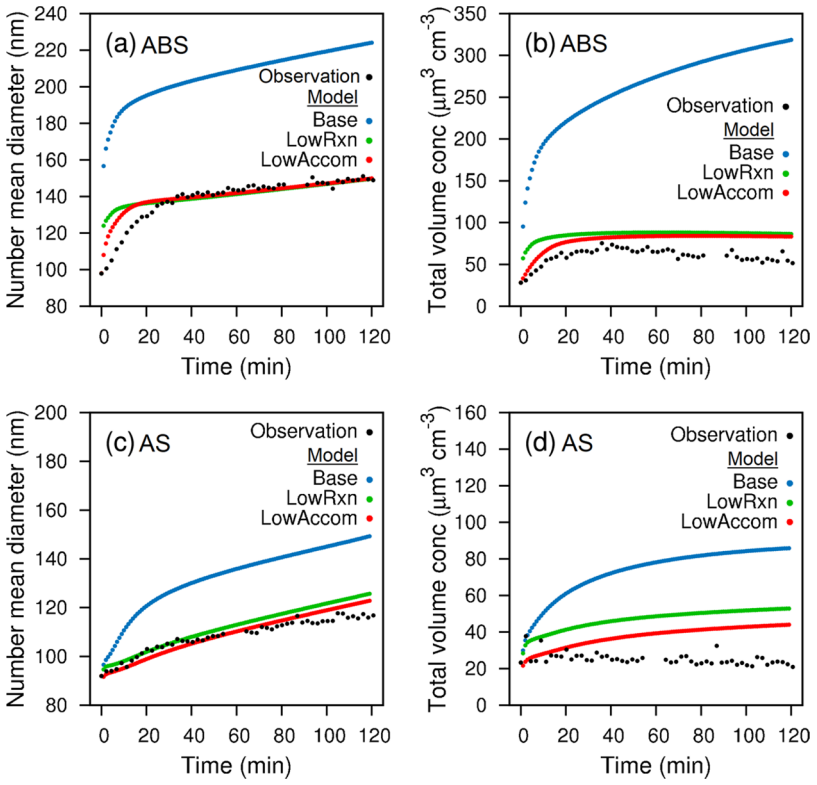


**Figure 2.** Time evolution of aerosol number mean diameter (left) and total suspended aerosol volume concentrations (right) from observations (black dots) and model simulations (color dots) with (a, b) ammonium bisulfate (ABS) seed aerosols and (c, d) ammonium sulfate (AS) seed aerosols. Since the model incorporates size-dependent loss of particles to the walls, measurements were not wall-loss-corrected for consistency with the model predictions. The slight decrease of total volume concentration of aerosols during IEPOX-SOA formation on AS seeds (d) is mainly caused by the size-dependent aerosol loss onto the chamber walls, which is mostly balanced by the increase of particle volume due to IEPOX-SOA formation.

treated based on Zaveri et al.[55] Semivolatile tetrols can be oligomerized to form nonvolatile tetrol oligomers in the aerosol phase with a first-order e-folding time scale ($\tau_{olig}$). The first-order oligomerization rate ($1/\tau_{olig}$) affects the fraction of semivolatile and nonvolatile contents in the IEPOX-SOA, which is constrained by the measured SOA composition at the end of experiments in this study. The OS formation consumes inorganic sulfate in the particles, and the inorganic and organic sulfates are therefore molar balanced in the model. The IEPOX-SOA forms a coating shell outside the inorganic core, limiting the further uptake of IEPOX.[18,20]

**MOSAIC Model Setup.** In this study, the IEPOX-SOA formation through the multiphase reactive uptake mechanism described above is implemented in the Model for Simulating Aerosol Interactions and Chemistry (MOSAIC)[55,56] to simulate the particle size evolution and SOA product compositions due to IEPOX uptake onto acidified and nonacidified sulfate seed aerosols from the two humid chamber experiments. The MOSAIC model has capabilities to treat the kinetics of gas- and aerosol-phase chemistry, aerosol thermodynamics and phase state, coagulation and condensation, and gas/particle wall loss. In each time step (1 s), the model dynamically partitions organic and inorganic species and calculates equilibrium aerosol water content and acidity in each particle size bin. In this study, we applied the moving-bin approach to predict particle size distribution evolution due to SOA formation from the uptake of IEPOX. Coagulation was ignored for simplicity.

The updated model was used to simulate 2 h chamber experiments after introducing IEPOX gas. The aerosol size distribution was represented using 205 size bins, with diameters from ∼1.1 to ∼1700 nm. The model was initialized with a gas-phase IEPOX concentration of 500 ppb and the seed aerosol size distribution measured by SMPS before IEPOX injection. The molar concentrations of $NH_4^+$ and $SO_4^{2-}$ in each size bin were calculated based on the measured suspended dry aerosol volume, assuming the density of seed particles is 1.77 g $cm^{-3}$. The density of IEPOX-SOA (tetrols, OSs, and oligomers) is estimated to be 1.5 g $cm^{-3}$ based on Cui et al.'s study,[19] which also agrees with Riva et al.'s measured density of overall particles (seed + IEPOX-SOA) at the end of experiment.[43] The MW for tetrols and OSs were assumed as 136 and 216 g $mol^{-1}$, respectively. The MW for tetrol oligomers in this study is treated as the hemiacetal dimer of 2 tetrol molecules, which has an MW of 254 g $mol^{-1}$ as proposed in Surratt et al.'s studies.[17,54]

We explicitly applied gas- and particle-phase chamber wall losses in the box model. The particle loss onto the chamber walls was characterized by a size-dependent first-order deposition rate,[57] as described in Xing et al.'s study.[58] The detailed calculation steps are shown in Section S1 in the Supporting Information. The model-simulated total suspended particle number generally agrees with the chamber periodical measurements for both ABS and AS seed aerosols (see Figure S1 in the Supporting Information). The gas-phase wall loss follows the methods described by He et al.,[59] which have been used in the box modeling of several chamber experiments.[60−62]


https://doi.org/10.1021/acsearthspacechem.2c00358
ACS Earth Space Chem. XXXX, XXX, XXX−XXX

Briefly, the first-order uptake and release of vapors to the chamber walls were considered in the model using absorptive partitioning theory.[63,64] The C* for tetrols is assumed to be ~10 $\mu$g m$^{-3}$, and the loss of tetrols on chamber walls is not negligible. However, IEPOX is highly volatile with a C* estimation of $10^4$ $\mu$g m$^{-3}$, which is 3 orders of magnitude higher than the tetrols,[22,36] and the chamber wall loss for IEPOX shows little effect on modeling results. The effects of vapor wall loss are discussed later in the section below. The detailed calculations of gas- and particle-phase wall losses are included in Section S2 in the Supporting Information.

## RESULTS AND DISCUSSION

IEPOX-SOA formation depends on many uncertain parameters that relate to reaction rates and diffusion within the particle phase. By concurrently using several measurements during IEPOX-SOA formation in the chamber, we achieve good constraints on key parameters as described below. In addition to the measured growth of particle size distribution, we use measured volatility, particle composition, OS content, and density together to obtain model-measurement agreement. This provides unique insights into the processes governing IEPOX-SOA formation.

**Constraining the Aqueous-Phase Reaction Rate Kinetics.** The particle number mean diameter represents the number weighted average of dry aerosol midpoint diameter for each size bin in the chamber, which indicates the particle growth with the IEPOX reactive uptake. As IEPOX-SOA forms, the observed aerosol mean diameter increases by ~50% from 97.9 to 148.9 nm within 2 h of the experiments with ABS seeds, while it only increases by ~27% (91.9−116.8 nm) with AS seeds, indicating slower growth kinetics due to lower acidity of AS compared to ABS seed aerosols (as black dots in Figure 2a,c). With ABS seed aerosols, the total volume concentration of suspended dry aerosols increases from 28 $\mu$m$^3$ cm$^{-3}$ before injection of IEPOX to above 70 $\mu$m$^3$ cm$^{-3}$ in ~40 min, then it starts slightly decreasing to ~50 $\mu$m$^3$ cm$^{-3}$ after 2 h due to the particle wall loss (Figure 2b). However, there is no significant change in total volume concentration (25 ± 3 $\mu$m$^3$ cm$^{-3}$) in the experiment with AS seed aerosols (Figure 2d), where the slow particle growth is likely compensated by the particle loss onto the chamber walls.

The *Base* cases in Figure 2 (blue dots) were simulated based on the reaction rate constants and accommodation coefficient ($\alpha$ = 0.02) as described in Table 1, which is commonly used in IEPOX-SOA modeling studies.[36,38,44] In our previous study, this set of parameters resulted in reasonable agreement between predicted and measured particle size evolution and product composition under low-RH conditions with acidic ABS seed aerosols.[45] However, the base model with default parameters greatly overpredicts aerosol mean diameters and total volume concentrations for both ABS and AS seed aerosols under 50−60% RH conditions. To achieve a better model-measurement agreement, we had to reduce the reaction rate constants forming tetrols (when water is the nucleophile) by a factor of 4 in the simulation with ABS seeds (as *LowRxn* with green dots in Figure 2a,b). Since the total simulated IEPOX-SOA is the sum of organosulfates (sulfate is the nucleophile) and tetrols, the reduction of tetrol reaction rate increases the relative reaction rate ($\beta$) of OS in the total IEPOX-SOA formation from 0.17 in the *Base* case to 0.45 in the *LowRxn* case (see Figure S2a). At 2 h, the simulated number mean diameter and total volume concentration are 149.7 nm and 86.4 $\mu$m$^3$ cm$^{-3}$, respectively, and agree better with the measurements. For the simulation with AS seeds, in addition to slowing down the tetrol formation reactions by a factor of 5, the rate constant for the OS formation had to be reduced as well by multiplying it with a factor of 0.15 (as *LowRxn* with green dots in Figure 2c,d). The simulated particle number mean diameter and total volume concentration at 2 h are 125.7 nm and 52.9 $\mu$m$^3$ cm$^{-3}$, respectively, which are much lower than those in the *Base* case (~149.3 nm and ~85.8 $\mu$m$^3$ cm$^{-3}$, respectively). As shown in Figure S2b, the $\beta$ is estimated to be 0.22 in the *LowRxn* case, which is close to that in the *Base* case ($\beta$ = 0.18). The model-simulated IEPOX uptake coefficient ($\gamma_{IEPOX}$) for ABS is higher than that for AS by a factor of ~2, which is consistent with the acidity-dependent $\gamma_{IEPOX}$ shown in Gaston et al.[40]

The reaction rate constants used in the *Base* case were measured in the bulk solutions,[39] which could be significantly different from the uptake of IEPOX onto atmospheric aerosols. As discussed by Shrivastava et al.,[65] the production rate of IEPOX-SOA is characterized as the product of a reaction probability for IEPOX and a yield describing the fraction of that uptake that results in SOA mass, which is <15% determined by the laboratory work.[66] In addition to achieving better agreement with the chamber measurements, the reduced rate constant for tetrols is also consistent with model sensitivity simulations in Pye et al., which indicated that $k_{H^+} = 2 \times 10^{-4}$ M$^{-2}$ s$^{-1}$ leads to the best agreement with the field observations.[34]

**IEPOX Mass Accommodation Coefficient.** For all simulations with ABS and AS seed aerosols, the model-simulated particle growth much faster than the observations at the beginning of the experiment, as the blue and green dots in Figure 2. In the beginning, particle growth is greatest due to ample gas-phase IEPOX, the particle is purely inorganic with both sulfate and water, and there is no viscous organic shell of IEPOX-SOA to limit IEPOX uptake due to particle-phase diffusion limitations. The mass accommodation coefficient, representing the fraction of collisions, which result in a gas-phase molecule entering the particle,[67] influences the initial particle growth by governing the $\gamma_{IEPOX}$ calculation in the first several seconds with the extended resistor-based model represented by eq 2.[48]

Figure S3 shows the predicted overall resistance to mass transfer represented by $1/\gamma_{IEPOX}$ within the first 5 min of the simulation in a given aerosol size bin with the initial diameter of 68.6 nm, which has the highest aerosol seed concentration. The gas-phase diffusion resistor term has little effect on the $1/\gamma_{IEPOX}$ with a low value of ~0.3 compared to the other two terms, since gas-phase diffusion is much faster than particle-phase reaction and diffusion. The bulk-phase resistor term includes resistances from particle-phase diffusion and chemical reaction of IEPOX. For the ABS seeds, this term increases from ~167 to ~6600 within 5 min, and it becomes the dominant factor in determining the $1/\gamma_{IEPOX}$ afterward. However, at the beginning of simulations, the $1/\gamma_{IEPOX}$ is significantly influenced by the accommodation coefficient ($1/\alpha$). With the assumed $\alpha$ of 0.02 ($1/\alpha$ = 50.0), the $1/\gamma_{IEPOX}$ starts from ~220 for ABS seeds, resulting in the high uptake coefficient $\gamma_{IEPOX} = 4.6 \times 10^{-3}$. When we reduced the $\alpha$ by an order of magnitude to $10^{-3}$ ($1/\alpha = 10^3$), the $\gamma_{IEPOX}$ is reduced effectively to $10^{-3}$ ($1/\gamma_{IEPOX} = 10^3$) and decreases the model overpredictions in the initial particle growth, bringing model predictions into closer agreement with measurements. In


https://doi.org/10.1021/acsearthspacechem.2c00358
ACS Earth Space Chem. XXXX, XXX, XXX−XXX

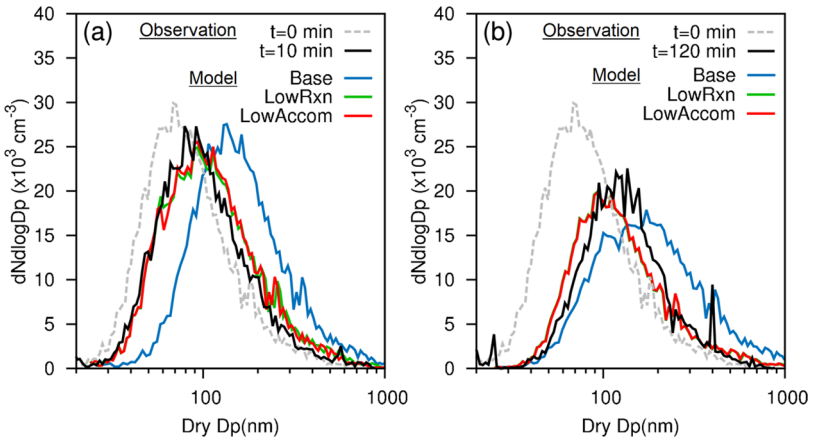


**Figure 3.** Size distribution evolution of aerosol number concentration of observations (black lines) and model simulations (color lines) at (a) 10 min and (b) 120 min from the start of introducing IEPOX gas (gray dashed lines) onto ABS aerosols.

contrast for the AS seeds, the bulk-phase resistor term of ~5.0 × $10^4$ is 2 orders of magnitude higher than ABS seeds at the beginning of the experiment and governs overall resistance to mass transfer ($1/\gamma_{IEPOX}$). The high bulk resistor term for AS seeds is mainly because of slower reaction kinetics in AS seeds compared to acidic ABS seeds. Therefore, reducing the accommodation coefficient has little impact on the overall resistance to mass transfer ($1/\gamma_{IEPOX}$) for AS seeds.

The fast initial growth for the ABS simulations is thus contributed by the high accommodation coefficient ($\alpha$ = 0.02) in the *LowRxn* case, although $\alpha$ = 0.02 is commonly used in the current models. An even higher value of $\alpha$ = 0.1 has been suggested by Gaston et al.[40] Octaviani et al.[45] showed that the model is sensitive to the mass accommodation coefficient of IEPOX, and a higher value of 0.1 leads to better particle growth evolution under dry and acidic conditions at 2 h, but this $\alpha$ = 0.1 overpredicts the initial growth of particles under dry conditions. In this study, we applied a low accommodation coefficient of $10^{-3}$ in the model to improve the model performance in particle evolution (see *LowAccom* with red dots in Figure 2). A low value of the surface accommodation coefficient $\alpha$ represents the physical process of mixing between IEPOX gas and seed aerosols in the chamber in addition to the uptake of IEPOX to the particles. The large ratio of IEPOX gas concentration to the seed aerosols could significantly increase the mixing timescales and reduce the fraction of an IEPOX molecule entering the particle at the beginning of the experiment. However, as discussed above, the particle growth after the first 5 min for ABS is mostly governed by the particle-phase diffusion-reactive term and not by the accommodation coefficient.

For the ABS seed aerosol experiment, with a lower mass accommodation coefficient, the initial particle growth is slower and closer to the observations, but the particle number mean diameter and total volume concentration have little changes at 2 h (149.9 nm and 83.3 $\mu m^3$ $cm^{-3}$, respectively) compared to the *LowAccom* case (Figure 2a,b). That is because the inorganic sulfates ($SO_4^{2-}$ + $HSO_4^-$) were nearly consumed and converted to nonvolatile OSs at the end of the simulation[20] (see Figure S4a). For the less acidic AS seed aerosol experiment, the lower mass accommodation coefficient ($\alpha$ = 0.001) improves the model-measurement agreement of the particle size evolution significantly, with the 2 h predicted number mean diameter of 122.8 nm and total volume concentration of 44.0 $\mu m^3$ $cm^{-3}$ that are close to the observations (116.8 nm and 21.3 $\mu m^3$ $cm^{-3}$, respectively, as Figure 2c,d). Due to the lower acidity of AS seed aerosols compared to ABS, particle-phase reaction rates are slower in AS seed aerosol experiment, resulting in higher resistance to the IEPOX mass transfer (see Figure S3). Therefore, with a slower rate of OS formation, only half of the inorganic sulfates were consumed and converted to OS, and the particle keeps growing with the continuous formation of IEPOX-SOA (see Figure S4b). The particle growth during the entire simulation is controlled by the bulk-phase resistor regardless of the $\alpha$ value. Thus, the particle evolution during the entire simulation is not very sensitive to the mass accommodation coefficient. The *LowAccom* cases agree well with chamber-measured number mean diameters, but slightly overpredict the total aerosol volume concentrations, especially for AS aerosols. The decrease in total volume concentration is mainly governed by the size-dependent loss of aerosols onto the chamber walls. Although our model includes size-dependent particle wall loss for the chamber based on Xing et al.,[58] its representation is likely more uncertain for the AS seed aerosol experiment compared to ABS seed aerosols (see Figure S1). The slight overprediction of particle distribution in the larger particle size bins at the end of simulation (as shown in Figure S6b) contributes to the higher model-simulated total volume concentrations compared to the observations (Figure 2d).

**Evolution of IEPOX Uptake Coefficient.** The IEPOX uptake coefficient ($\gamma_{IEPOX}$) is treated as a time-dependent variable, which is estimated based on the extended resistor-based model described in Anttila et al.[48] Figure S5a shows the simulated time evolution of $\gamma_{IEPOX}$ in a given aerosol size bin with the initial diameter of 68.6 nm during the simulated time of 2 h. The model-simulated $\gamma_{IEPOX}$ for ABS is much higher than that for AS at the beginning of the experiment, which is consistent with the acidity-dependent $\gamma_{IEPOX}$ shown in Gaston et al.[40] The $\gamma_{IEPOX}$ in the ABS simulation continuously decreases from its initial value of 1 × $10^{-3}$ to 2 × $10^{-6}$ at the end of simulation. The initial value is lower than that of previous studies[40,42] because a lower mass accommodation coefficient ($\alpha$ = $10^{-3}$) was applied in the model to limit the uptake of IEPOX at the beginning of simulation that implicitly accounts for the initial gas-particle mixing limitations in the chamber and achieves model-measurement agreement. In contrast, the simulated $\gamma_{IEPOX}$ in the AS simulation rapidly


https://doi.org/10.1021/acsearthspacechem.2c00358
ACS Earth Space Chem. XXXX, XXX, XXX−XXX

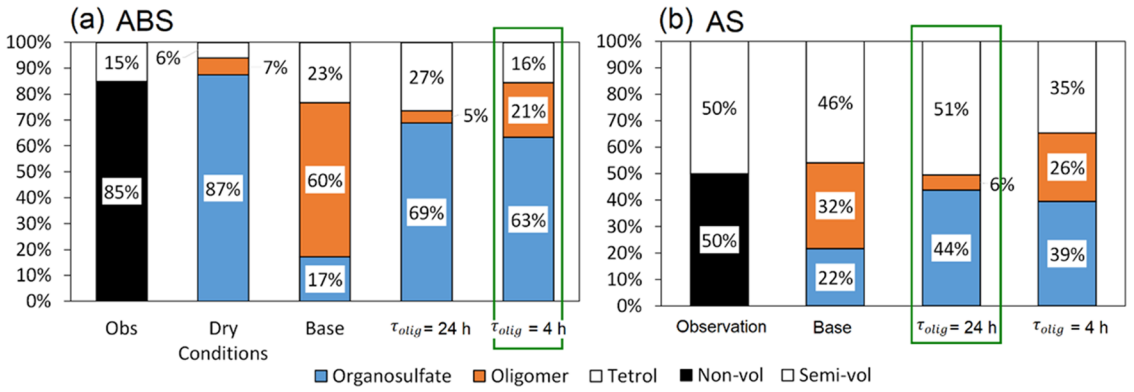


**Figure 4.** Relative mass contributions of observed (nonvolatile and semivolatile) and simulated IEPOX-derived SOA compositions (OS, tetrols, and oligomers) at 2 h of simulations with (a) ABS aerosols and (b) AS aerosols. The dry-condition case refers to the simulation by Octaviani et al.[45] The simulations within the green box show the best agreement with the observations. The OS could possibly contain the monomer as well as the dimers and trimers in the measurements, but they are not explicitly modeled in this study.

increases to its highest value of $\sim 5 \times 10^{-5}$ in the first 10 min due to the evaporation of $NH_4^+$, which leads to the increase of $H^+$ concentration (Figure S5b). $\gamma_{IEPOX}$ then slightly decreases to $\sim 2 \times 10^{-5}$, a value that is consistent with the $\gamma_{IEPOX}$ for AS reported by Gaston et al.[40] The reduction of $\gamma_{IEPOX}$ is mainly caused by the consumption of acids and nucleophiles, which increases the resistor term for aqueous reactions ($\Gamma_{aq}$) as shown in Figure S5c,d. Under 50−60% RH, the resistor term for coating ($\Gamma_{coat}$) that represents particle-phase diffusion limitations within the organic coating is lower than the $\Gamma_{aq}$ by several orders of magnitude, indicating that the self-limiting coating effects are small compared to the reactions under 50−60% RH, which is consistent with the 50% RH results in Zhang et al.[42]

**Size Distribution Evolution of Aerosol Number Concentrations.** The size distribution of aerosol number concentrations (d*N*/dlog Dp) at 10 and 120 min after IEPOX injection into the chamber with ABS seed aerosols are shown in Figure 3. The measured initial particle size distributions are unimodal and dominated by the particles in the range of 55−110 nm (25−75%), shown as the gray dashed lines. The observed particles at 10 and 120 min predominantly lie in the range of 65−135 and 90−170 nm, respectively (black lines). Model calculations in the base case (blue lines) predict the particles grow much faster than the observations and are mostly distributed in the larger particle size ranges at 10 and 120 min (107−227 and 110−290 nm, respectively). After reducing the reaction rate constants for tetrol formation, the evolution of particle size distributions at 10 and 120 min are well captured, and the particle sizes are within the range of (69−160 and 80−163 nm). The final 2 h particle size distributions do not change with different IEPOX mass accommodation coefficients of 0.001 and 0.02.

The evolution of particle size distribution with AS seed aerosols is slower than that with ABS aerosols. The dominant particle number distribution range grows from 53−105 to 55−110 nm within ∼10 min and 73−135 nm at 120 min (i.e., at the end of the experiment), as shown in Figure S6. Similar to the simulation with ABS seed aerosols, the particles in the base case are predicted to grow faster and reach larger sizes compared to measurements during the entire simulation. Model cases with reduced reaction rate constants (as *LowRxn* and *LowAccom* described in Table 1) show better agreement with the observations (see green and red lines in Figure S6). The higher IEPOX accommodation coefficient of 0.02 leads to the faster initial growth of smaller particles, resulting in a narrower distribution, which is consistent with the finding in Octaviani et al.[45] At the end of simulations (120 min), the dominant particle number distributions lie within the range of 70−145 and 68−135 nm for *LowRxn* and *LowAccom* cases, respectively. The area under the number distribution curve but above the horizontal axis represents the total aerosol number in the chamber, and it shows that the model-simulated particle numbers agree well with the observed data.

A recent study shows that the $C_5$-alkene triols could be formed through the acid-driven IEPOX isomerization with a total yield of 7.6% (5% gas-phase yield and 2.5% particle-phase yield).[68] Although alkene triol formation is not included in this study, a 2.5% yield of particle-phase alkene triols is minor and cannot explain the four to five times overprediction of particle volume in the base case. In this work, we showed that a factor of 5 slower reaction kinetics compared to those derived by bulk solution measurements previously,[39] are needed to explain IEPOX-SOA formation on ABS and AS seeds.

**Potential Acidity-Dependent Oligomerization Timescale for Tetrols.** Particle-phase acidity is known to affect the oligomer formation of SOA particles.[65] However, the role of acidity in the oligomerization of IEPOX-SOA components is not well characterized. FIGAERO-CIMS measurements by D'Ambro et al.[22] suggested that IEPOX-derived semivolatile tetrols form nonvolatile oligomers through a first-order reaction time scale ($\tau_{olig}$) of a few hours. In the simulation of IEPOX reactive uptake under dry conditions, Octaviani et al.[45] adopted $\tau_{olig}$ of 2 h, based on D'Ambro et al.,[22] and predicted that approximately 50% of tetrols were oligomerized. Their model prediction agreed with the measured volatility of IEPOX-SOA. We varied the modeled $\tau_{olig}$ ranging 2−24 h to evaluate how the IEPOX-SOA composition and volatility changes with $\tau_{olig}$. All other parameters are the same as given in *LowAccom* case (see Table 1). Figure S7 shows that the simulated particle growth and size distribution evolution is not sensitive to the $\tau_{olig}$. However, $\tau_{olig}$ significantly affects the product volatility and composition, as shown in Figure S8. At the end of the chamber experiment, the observed volatility of IEPOX-SOA is used to constrain the oligomerization time scale in this study.

The miniSPLAT measurements indicate that ∼85% of IEPOX-SOA was nonvolatile when it was formed on ABS


https://doi.org/10.1021/acsearthspacechem.2c00358
ACS Earth Space Chem. XXXX, XXX, XXX−XXX

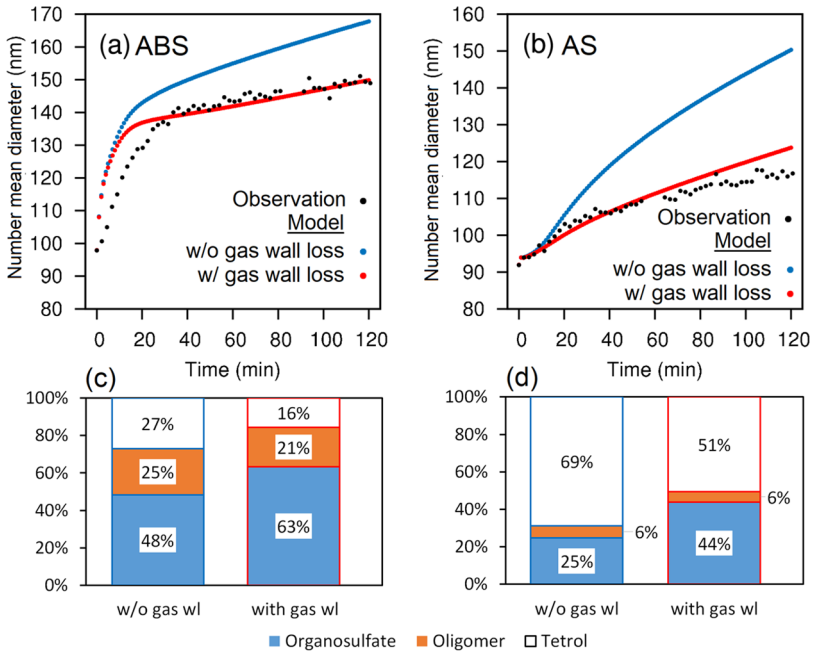


**Figure 5.** Impacts of tetrol gas wall loss on the time evolution of (a) aerosol number mean diameter (nm) and (b) total suspended aerosol volume concentrations, and relative mass contributions of simulated IEPOX-SOA compositions at 2 h.

seeds; however, only ∼50% was nonvolatile on AS seeds (Figure 4). In our model, the sum of OSs and Tetrol oligomers constitutes the nonvolatile fraction of IEPOX-SOA with the remaining fraction attributed to the remaining particle-phase nonoligomerized semivolatile tetrols. For IEPOX-SOA formation on ABS seeds, the base case model predicts only 74% nonvolatile components compared to the observed fraction of 85%, and only 13% is OSs, which is inconsistent with the measurements by Riva et al.[43] RPLC/ESI-HR-QTOFMS measurements by Riva et al.[43] indicated that ∼40% of IEPOX-SOA is OSs, and GC/EI-MS measurements indicated that ∼30% is $C_5$-alkene triols. Frauenheim et al. found that ∼10−50% of $C_5$-alkene triols are formed through acid-driven particle-phase IEPOX isomerization,[68] and the rest of them are believed to be analytical artifacts and suggested to be decomposition products from OSs that were not measured.[22] Therefore, ∼40−70% of IEPOX-SOA are likely OSs. By reducing the reaction rate constants for tetrols in the model, we predict a reasonable OS fraction in the range of 64−73% (see Figure S8a). Varying the simulated tetrol oligomerization timescales in the model results in the predicted nonvolatile SOA components ranging from 77 to 91%. With $\tau_{olig}$ = 4 h, the modeled fraction of nonvolatile content (84%) shows best agreement with the observation (85%). The predicted fraction of total tetrols (tetrols + oligomers) comprises 37% of IEPOX-SOA, which is a factor of 3 higher than that in the simulation of dry-condition experiment (see Figure 4a),[45] and is also consistent with miniSPLAT and GC/EI-MS measurements.[43]

For IEPOX uptake onto AS seed aerosols, the base case model predicts 54% nonvolatile products at the end of the simulation, which is in good agreement with the miniSPLAT measurements of ∼50% nonvolatile content. GC/EI-MS measurements indicated that ∼50% of IEPOX-SOA is OS, which indicates that the miniSPLAT observed nonvolatile components can mostly be attributed to nonvolatile OSs. Although the base case simulation provides a reasonable fraction of total nonvolatile content, it predicts that the tetrol oligomers are dominant in the nonvolatile components, which cannot explain the GC/EI-MS measurements. To increase the predicted fraction of OSs, we needed to reduce the reaction rate coefficients for both tetrols and OSs formation by a factor of ∼5 and reduce the oligomerization timescale of tetrols. Figure S8b shows that with higher oligomerization timescales ($\tau_{olig}$ > 16 h), the predicted nonvolatile fraction is ∼50% and the tetrol oligomers fraction is less than 10%. The model with $\tau_{olig}$ = 24 h in this study predicted 49.5% nonvolatile content, which is dominated by OSs (44%), and it agrees best with the observed product composition.

The measurements of product composition at the end of the experiments constrain the tetrol oligomerization time scale. To explain the measured IEPOX-SOA composition and nonvolatile content of IEPOX-SOA, our model indicates that a factor of ∼6 faster oligomerization rate for more acidic ABS seed aerosols ($\tau_{olig}$ of 4 h) compared to AS seeds ($\tau_{olig}$ of 24 h), resulting in the oligomerization rate ($1/\tau_{olig}$) of ∼$6.9 \times 10^5$ and $1.2 \times 10^5$ $s^{-1}$, respectively. The variation of oligomerization rate is most likely controlled by varying acidities of seed aerosols. AS seeds have initial pH of ∼1.5 with little variation during the entire simulation, while with ABS seeds, the IEPOX uptake process increases the particle pH from the initial value of negative (−) 0.9 to ∼1.3 within ∼30 min, which is driven by the conversion of inorganic sulfates to OSs.[18,20] An even lower $\tau_{olig}$ = 2 h was adopted in Octaviani et al.'s simulation of IEPOX uptake onto acidified ABS seed aerosols under dry conditions (5% RH compared to 50−60% RH in this study). Under dry conditions, ABS seed aerosols exist in metastable states that contain a small amount of aerosol water[69] and have an initial pH of −3.43,[45] higher acidity compared to the 50−60% RH in this study. Combining the simulations under dry and wet conditions with varying seed particle acidities, the tetrol oligomerization process is potentially catalyzed by particle acidity and the oligomerization rate is likely faster with lower aerosol pH, consistent with prior work.[70]


https://doi.org/10.1021/acsearthspacechem.2c00358
ACS Earth Space Chem. XXXX, XXX, XXX−XXX

**Effects of Tetrol Gas Wall Loss.** In this study, the vapor wall loss for both IEPOX and tetrol gases is treated as a kinetic process, which is described in Section S2 in the Supporting Information. Semivolatile gases like tetrols are more efficiently lost to chamber walls compared to more volatile gases like IEPOX. Gas-phase wall loss was not included in Octaviani et al.'s simulation of the dry-chamber experiment due to its limited effects on the particle size evolution,[45] which is likely caused by the little semivolatile tetrols formed under low RH (~5%). In our prior study, ~90% of IEPOX-SOA was predicted to be OSs. However, under the higher RH experiments of 50−60% in our study, tetrols constitute a larger fraction of IEPOX-SOA as indicated by miniSPLAT, GC/EI-MS measurements, and our model. Vapor loss onto the chamber walls reduces the concentrations of tetrols in the gas phase and causes more tetrols to partition to the gas phase to achieve gas-particle equilibrium. This in turn also reduces their oligomerization process. We assessed the effects of gas-phase wall loss on particle size evolution and product composition for the ABS and AS seed aerosols under humid conditions by comparing model simulations with gas-phase wall loss on (w/ gas wall loss) and off (w/o gas wall loss), as shown in Figure 5. All other parameters are the same as given in *LowAccom* case in Table 1. Compared to all other cases that have wall loss on, as presented in this manuscript, turning gas-phase wall loss off results in 15−21% overprediction in the number mean diameters of particles (Figure 5a,b). In addition, the fractions of total tetrol products (tetrols + oligomers) are predicted to increase by 11 and 19% for ABS and AS seed aerosols, respectively, and the fractions of semivolatile content in IEPOX-SOA (27% for ABS and 69% for AS) are significantly higher than the observations (16% for ABS and 51% for AS, Figure 5c,d). In summary, including gas-phase wall loss improves model-measurement agreement.

## CONCLUSIONS

In this study, we applied the MOSAIC box model with several updates to the IEPOX-SOA formation scheme to simulate the environmental chamber experiments of IEPOX reactive uptake on acidified and nonacidified seed aerosols under 50−60% RH conditions. Constrained by the chamber-measured particle size evolution and IEPOX-SOA product compositions and volatility, the model simulations provided new insights into the IEPOX reactive uptake process. The aqueous-phase acid-driven reaction rate constants in the base case model, which were derived from bulk solution kinetics and used in all previous models, greatly overpredict the IEPOX-SOA formation under 50−60% RH conditions. By reducing the particle-phase tetrol formation reaction rate constants by a factor of 4, the evolutions of the number mean diameter and total aerosol volume concentration with acidified sulfate seeds were brought into much better agreement with the chamber observations. The simulated branching ratio ($\beta$) of OS formation is approximately 0.45 for ABS seeds under 51% RH conditions. For less acidic AS seeds, in addition to reducing the tetrol reaction rates by a factor of 5, the OS reaction rate constant needed to be reduced by multiplying it with a factor of 0.15 to explain measured particle composition including the OS content and volatility. In contrast, all current CTMs use the same aqueous reaction rate constants to simulate IEPOX-SOA formation irrespective of acidity and RH, which could significantly bias their predictions of tetrols and OSs formed under elevated-RH conditions. Our study shows that IEPOX-SOA reaction rates within atmospheric aerosols strongly depend on RH and seed particle acidity. The implication is that chemical kinetics derived from bulk solution measurements used in previous studies are most likely a factor of 4−5 too high compared to the kinetics needed to explain IEPOX-SOA formation on actual atmospheric aerosols, as shown in this study.

We also show that the tetrol oligomerization process that affects the volatility and composition of SOA products reveals a strong dependence on seed aerosol acidity. We constrain this oligomerization rate using the miniSPLAT measurements of IEPOX-SOA volatility and GC/EI-MS measured components, especially the fraction of OS. We find that an oligomerization time scale of 4 h best matches measurements in simulating IEPOX uptake onto acidified seeds (pH = −0.9 to 1.3), while a much longer time scale of 24 h is suitable for less acidic AS seeds (pH ~ 1.5). An oligomerization time of 2 h was used for acidified seed aerosols under dry conditions, which have even higher acidities (pH = −3.4 to −0.5).[45] Based on the three experiments with varying seed aerosol acidities, we show that the oligomerization process is faster on the aerosols with higher acidities (lower pH) and under drier conditions. The dependence of aerosol acidity on the tetrol oligomerization rate should be more carefully investigated by well-designed experiments in the future.

To simulate IEPOX-SOA formation in the elevated-RH chamber experiment, we show that the semivolatile tetrol loss onto the walls was significant. When the tetrol gas wall loss was turned off, our model overpredicted the evolution of particle size and the tetrol fractions in IEPOX-SOA. We also showed that the mass accommodation coefficient for IEPOX significantly impacts the predicted particle initial growth for ABS seeds during the initial stages of particle growth, but not for AS seeds. Initial particle growth for AS seeds is mainly governed by particle-phase chemical kinetics that is much slower than ABS seeds.

Our results imply that IEPOX reactive uptake kinetics used in regional and global models, which are based on bulk aqueous solution measurements have likely overpredicted IEPOX-SOA formation from aqueous chemistry in the atmosphere. Models that consider the updated reaction rate coefficients and tetrol oligomerization rates, which are RH- and acidity-dependent, as derived in this work, could help derive critical insights about key processes governing IEPOX-SOA formation in the atmosphere. Getting the right answers for the right reasons is critical for identifying gaps in our current understanding of aqueous-phase SOA formation, and process discovery through model-measurement comparisons, as highlighted in our recent study.[36] Although the RH of 50−60% investigated in this study is commonly considered representative of elevated-RH conditions in recent chamber experiments,[71,72] it is still below the relative humidity levels near the earth's surface at several locations in the atmosphere (e.g., greater than 70% RH during the wintertime).[73] The parameters (i.e., reaction rate constants) under higher RH conditions need to be further validated by experimental measurements and modeling studies in the future.

## ASSOCIATED CONTENT

### Supporting Information

The Supporting Information is available free of charge at https://pubs.acs.org/doi/10.1021/acsearthspacechem.2c00358.



https://doi.org/10.1021/acsearthspacechem.2c00358
ACS Earth Space Chem. XXXX, XXX, XXX−XXX

Size-dependent particle wall loss (Section S1), gas-phase chamber wall loss (Section S2), time evolution of organosulfate branching ratio (Figure S2), model predicted resistance to mass transfer (Figure S3), time series concentrations of aerosol components in the chamber (Figure S4), time evolution of IEPOX uptake coefficient (Figure S5), size distribution evolution of aerosol number concentration for AS aerosols (Figure S6), time evolution of number mean diameter and aerosol size distribution with different oligomerization timescales (Figure S7), sensitivity of relative mass fractions on tetrol oligomerization time scale (Figure S8), and references (PDF)

## AUTHOR INFORMATION


### Corresponding Author

**Manish Shrivastava** − *Pacific Northwest National Laboratory, Richland, Washington 99352, United States;* orcid.org/0000-0002-9053-2400; Email: manishkumar.shrivastava@pnnl.gov

### Authors

**Jie Zhang** − *Pacific Northwest National Laboratory, Richland, Washington 99352, United States*

**Alla Zelenyuk** − *Pacific Northwest National Laboratory, Richland, Washington 99352, United States*

**Rahul A. Zaveri** − *Pacific Northwest National Laboratory, Richland, Washington 99352, United States;* orcid.org/0000-0001-9874-8807

**Jason D. Surratt** − *Department of Environmental Sciences and Engineering, Gillings School of Global Public Health, University of North Carolina at Chapel Hill, Chapel Hill, North Carolina 27599, United States; Department of Chemistry, College of Arts and Sciences, University of North Carolina at Chapel Hill, Chapel Hill, North Carolina 27599, United States;* orcid.org/0000-0002-6833-1450

**Matthieu Riva** − *IRCELYON, Université Lyon, Université Claude Bernard Lyon 1, CNRS, 69626 Villeurbanne, France;* orcid.org/0000-0003-0054-4131

**David Bell** − *Laboratory of Atmospheric Chemistry, Paul Scherrer Institute, Villigen 5232, Switzerland;* orcid.org/0000-0002-3958-2138

**Marianne Glasius** − *Department of Chemistry, Aarhus University, 8000 Aarhus C, Denmark;* orcid.org/0000-0002-4404-6989

Complete contact information is available at: https://pubs.acs.org/10.1021/acsearthspacechem.2c00358


### Notes

The authors declare no competing financial interest.

## ACKNOWLEDGMENTS

This research was supported by the U.S. Department of Energy (DOE) Office of Science, Office of Biological and Environmental Research (BER) through the Early Career Research Program. Computational resources for the simulations were provided by EMSL (a DOE Office of Science User Facility sponsored by the Office of Biological and Environmental Research located at PNNL). R.A.Z. and A.Z. acknowledge support from the U.S. Department of Energy (DOE) Atmospheric System Research (ASR) program via the Integrated Cloud, Land-surface, and Aerosol System Study (ICLASS) Science Focus Area at PNNL. Pacific Northwest National Laboratory (PNNL) is operated for DOE by the Battelle Memorial Institute under contract no. DE-A05-76RLO1830. J.D.S. acknowledges funding from the National Science Foundation (NSF) under Atmospheric and Geospace (AGS) Grant 2039788.

## REFERENCES


(1) Guenther, A.; Karl, T.; Harley, P.; Wiedinmyer, C.; Palmer, P. I.; Geron, C. Estimates of global terrestrial isoprene emissions using MEGAN (Model of Emissions of Gases and Aerosols from Nature). *Atmos. Chem. Phys.* **2006**, *6*, 3181−3210.

(2) Carlton, A. G.; Wiedinmyer, C.; Kroll, J. A review of Secondary Organic Aerosol (SOA) formation from isoprene. *Atmos. Chem. Phys.* **2009**, *9*, 4987−5005.

(3) Kroll, J. H.; Ng, N. L.; Murphy, S. M.; Flagan, R. C.; Seinfeld, J. H. Secondary organic aerosol formation from isoprene photooxidation. *Environ. Sci. Technol.* **2006**, *40*, 1869−1877.

(4) Song, M.; Zhang, C.; Wu, H.; Mu, Y.; Ma, Z.; Zhang, Y.; Liu, J.; Li, X. The influence of OH concentration on SOA formation from isoprene photooxidation. *Sci. Total Environ.* **2019**, *650*, 951−957.

(5) Sato, K.; Inomata, S.; Xing, J.-H.; Imamura, T.; Uchida, R.; Fukuda, S.; Nakagawa, K.; Hirokawa, J.; Okumura, M.; Tohno, S. Effect of OH radical scavengers on secondary organic aerosol formation from reactions of isoprene with ozone. *Atmos. Environ.* **2013**, *79*, 147−154.

(6) Kleindienst, T. E.; Lewandowski, M.; Offenberg, J. H.; Jaoui, M.; Edney, E. O. Ozone-isoprene reaction: Re-examination of the formation of secondary organic aerosol. *Geophys. Res. Lett.* **2007**, *34*, No. L01805.

(7) Ng, N.; Kwan, A.; Surratt, J.; Chan, A.; Chhabra, P.; Sorooshian, A.; Pye, H. O.; Crounse, J.; Wennberg, P.; Flagan, R. Secondary organic aerosol (SOA) formation from reaction of isoprene with nitrate radicals (NO 3). *Atmos. Chem. Phys.* **2008**, *8*, 4117−4140.

(8) Suh, I.; Lei, W.; Zhang, R. Experimental and theoretical studies of isoprene reaction with NO3. *J. Phys. Chem. A* **2001**, *105*, 6471−6478.

(9) Hamilton, J. F.; Bryant, D. J.; Edwards, P. M.; Ouyang, B.; Bannan, T. J.; Mehra, A.; Mayhew, A. W.; Hopkins, J. R.; Dunmore, R. E.; Squires, F. A.; et al. Key role of NO3 radicals in the production of isoprene nitrates and nitrooxyorganosulfates in Beijing. *Environ. Sci. Technol.* **2021**, *55*, 842−853.

(10) Hu, W. W.; Campuzano-Jost, P.; Palm, B.; Day, D.; Ortega, A.; Hayes, P.; Krechmer, J.; Chen, Q.; Kuwata, M.; Liu, Y.; et al. Characterization of a real-time tracer for isoprene epoxydiols-derived secondary organic aerosol (IEPOX-SOA) from aerosol mass spectrometer measurements. *Atmos. Chem. Phys.* **2015**, *15*, 11807−11833.

(11) Jo, D. S.; Hodzic, A.; Emmons, L. K.; Marais, E. A.; Peng, Z.; Nault, B. A.; Hu, W.; Campuzano-Jost, P.; Jimenez, J. L. A simplified parameterization of isoprene-epoxydiol-derived secondary organic aerosol (IEPOX-SOA) for global chemistry and climate models: a case study with GEOS-Chem v11-02-rc. *Geosci. Model Dev.* **2019**, *12*, 2983−3000.

(12) Atkinson, R. Gas-phase tropospheric chemistry of volatile organic compounds: 1. Alkanes and Alkenes. *J. Phys. Chem. Ref. Data* **1997**, *26*, 215−290.

(13) Pandis, S. N.; Paulson, S. E.; Seinfeld, J. H.; Flagan, R. C. Aerosol formation in the photooxidation of isoprene and $\beta$-pinene. *Atmos. Environ., Part A* **1991**, *25*, 997−1008.

(14) Wennberg, P. O.; Bates, K. H.; Crounse, J. D.; Dodson, L. G.; McVay, R. C.; Mertens, L. A.; Nguyen, T. B.; Praske, E.; Schwantes, R. H.; Smarte, M. D.; et al. Gas-phase reactions of isoprene and its major oxidation products. *Chem. Rev.* **2018**, *118*, 3337−3390.

(15) Paulot, F.; Crounse, J. D.; Kjaergaard, H. G.; Kürten, A.; St Clair, J. M.; Seinfeld, J. H.; Wennberg, P. O. Unexpected epoxide formation in the gas-phase photooxidation of isoprene. *Science* **2009**, *325*, 730−733.

(16) Bates, K. H.; Crounse, J. D.; St Clair, J. M.; Bennett, N. B.; Nguyen, T. B.; Seinfeld, J. H.; Stoltz, B. M.; Wennberg, P. O. Gas phase production and loss of isoprene epoxydiols. *J. Phys. Chem. A* **2014**, *118*, 1237−1246.
(17) Surratt, J. D.; Chan, A. W.; Eddingsaas, N. C.; Chan, M.; Loza, C. L.; Kwan, A. J.; Hersey, S. P.; Flagan, R. C.; Wennberg, P. O.; Seinfeld, J. H. Reactive intermediates revealed in secondary organic aerosol formation from isoprene. *Proc. Natl. Acad. Sci. U.S.A.* **2010**, *107*, 6640−6645.
(18) Zhang, Y.; Chen, Y.; Lei, Z.; Olson, N. E.; Riva, M.; Koss, A. R.; Zhang, Z.; Gold, A.; Jayne, J. T.; Worsnop, D. R.; et al. Joint impacts of acidity and viscosity on the formation of secondary organic aerosol from isoprene epoxydiols (IEPOX) in phase separated particles. *ACS Earth Space Chem.* **2019**, *3*, 2646−2658.
(19) Cui, T.; Zeng, Z.; Dos Santos, E. O.; Zhang, Z.; Chen, Y.; Zhang, Y.; Rose, C. A.; Budisulistiorini, S. H.; Collins, L. B.; Bodnar, W. M.; et al. Development of a hydrophilic interaction liquid chromatography (HILIC) method for the chemical characterization of water-soluble isoprene epoxydiol (IEPOX)-derived secondary organic aerosol. *Environ. Sci.: Processes Impacts* **2018**, *20*, 1524−1536.
(20) Riva, M.; Chen, Y.; Zhang, Y.; Lei, Z.; Olson, N. E.; Boyer, H. C.; Narayan, S.; Yee, L. D.; Green, H. S.; Cui, T.; et al. Increasing isoprene epoxydiol-to-inorganic sulfate aerosol ratio results in extensive conversion of inorganic sulfate to organosulfur forms: implications for aerosol physicochemical properties. *Environ. Sci. Technol.* **2019**, *53*, 8682−8694.
(21) Lopez-Hilfiker, F. D.; Mohr, C.; D'ambro, E.; Lutz, A.; Riedel, T.; Gaston, C.; Iyer, S.; Zhang, Z.; Gold, A.; Surratt, J.; et al. Molecular composition and volatility of organic aerosol in the Southeastern US: implications for IEPOX derived SOA. *Environ. Sci. Technol.* **2016**, *50*, 2200−2209.
(22) D'Ambro, E. L.; Schobesberger, S.; Gaston, C. J.; Lopez-Hilfiker, F. D.; Lee, B. H.; Liu, J.; Zelenyuk, A.; Bell, D.; Cappa, C. D.; Helgestad, T.; et al. Chamber-based insights into the factors controlling epoxydiol (IEPOX) secondary organic aerosol (SOA) yield, composition, and volatility. *Atmos. Chem. Phys.* **2019**, *19*, 11253−11265.
(23) Jaoui, M.; Corse, E. W.; Lewandowski, M.; Offenberg, J. H.; Kleindienst, T. E.; Edney, E. O. Formation of organic tracers for isoprene SOA under acidic conditions. *Atmos. Environ.* **2010**, *44*, 1798−1805.
(24) Kleindienst, T. E.; Jaoui, M.; Lewandowski, M.; Offenberg, J. H.; Lewis, C. W.; Bhave, P. V.; Edney, E. O. Estimates of the contributions of biogenic and anthropogenic hydrocarbons to secondary organic aerosol at a southeastern US location. *Atmos. Environ.* **2007**, *41*, 8288−8300.
(25) Brüggemann, M.; Xu, R.; Tilgner, A.; Kwong, K. C.; Mutzel, A.; Poon, H. Y.; Otto, T.; Schaefer, T.; Poulain, L.; Chan, M. N.; Herrmann, H. Organosulfates in ambient aerosol: state of knowledge and future research directions on formation, abundance, fate, and importance. *Environ. Sci. Technol.* **2020**, *54*, 3767−3782.
(26) He, Q. F.; Ding, X.; Fu, X. X.; Zhang, Y. Q.; Wang, J. Q.; Liu, Y. X.; Tang, M. J.; Wang, X. M.; Rudich, Y. Secondary Organic Aerosol Formation From Isoprene Epoxides in the Pearl River Delta, South China: IEPOX-and HMML-Derived Tracers. *J. Geophys. Res.: Atmos.* **2018**, *123*, 6999−7012.
(27) Ding, X.; He, Q.-F.; Shen, R.-Q.; Yu, Q.-Q.; Zhang, Y.-Q.; Xin, J.-Y.; Wen, T.-X.; Wang, X.-M. Spatial and seasonal variations of isoprene secondary organic aerosol in China: Significant impact of biomass burning during winter. *Sci. Rep.* **2016**, *6*, No. 20411.
(28) Hughes, D. D.; Christiansen, M. B.; Milani, A.; Vermeuel, M. P.; Novak, G. A.; Alwe, H. D.; Dickens, A. F.; Pierce, R. B.; Millet, D. B.; Bertram, T. H.; et al. PM2. 5 chemistry, organosulfates, and secondary organic aerosol during the 2017 Lake Michigan Ozone Study. *Atmos. Environ.* **2021**, *244*, No. 117939.
(29) Chen, Y.; Dombek, T.; Hand, J.; Zhang, Z.; Gold, A.; Ault, A. P.; Levine, K. E.; Surratt, J. D. Seasonal Contribution of Isoprene-Derived Organosulfates to Total Water-Soluble Fine Particulate Organic Sulfur in the United States. *ACS Earth Space Chem.* **2021**, *5*, 2419−2432.
(30) Glasius, M.; Bering, M. S.; Yee, L. D.; de Sá, S. S.; Isaacman-VanWertz, G.; Wernis, R. A.; Barbosa, H. M.; Alexander, M. L.; Palm, B. B.; Hu, W.; et al. Organosulfates in aerosols downwind of an urban region in central Amazon. *Environ. Sci.: Processes Impacts* **2018**, *20*, 1546−1558.
(31) Zhang, J.; He, X.; Gao, Y.; Zhu, S.; Jing, S.; Wang, H.; Yu, J. Z.; Ying, Q. Estimation of aromatic secondary organic aerosol using a molecular tracer—a chemical transport model assessment. *Environ. Sci. Technol.* **2021**, *55*, 12882−12892.
(32) Ashraf, F.; Babar, Z. B.; Park, J.-H.; Dao, P. D. Q.; Cho, C. S.; Lim, H.-J. Determination of Volatility Parameters of Secondary Organic Aerosol Components via Thermal Analysis. *Atmosphere* **2022**, *13*, 709.
(33) Qin, M.; Wang, X.; Hu, Y.; Ding, X.; Song, Y.; Li, M.; Vasilakos, P.; Nenes, A.; Russell, A. G. Simulating biogenic secondary organic aerosol during summertime in China. *J. Geophys. Res.: Atmos.* **2018**, *123*, 11100−11119.
(34) Pye, H. O. T.; Pinder, R. W.; Piletic, I. R.; Xie, Y.; Capps, S. L.; Lin, Y.-H.; Surratt, J. D.; Zhang, Z.; Gold, A.; Luecken, D. J.; et al. Epoxide pathways improve model predictions of isoprene markers and reveal key role of acidity in aerosol formation. *Environ. Sci. Technol.* **2013**, *47*, 11056−11064.
(35) Budisulistiorini, S. H.; Li, X.; Bairai, S.; Renfro, J.; Liu, Y.; Liu, Y.; McKinney, K.; Martin, S.; McNeill, V.; Pye, H.; et al. Examining the effects of anthropogenic emissions on isoprene-derived secondary organic aerosol formation during the 2013 Southern Oxidant and Aerosol Study (SOAS) at the Look Rock, Tennessee ground site. *Atmos. Chem. Phys.* **2015**, *15*, 8871−8888.
(36) Shrivastava, M.; Rasool, Q. Z.; Zhao, B.; Octaviani, M.; Zaveri, R. A.; Zelenyuk, A.; Gaudet, B.; Liu, Y.; Shilling, J. E.; Schneider, J.; et al. Tight Coupling of Surface and In-Plant Biochemistry and Convection Governs Key Fine Particulate Components over the Amazon Rainforest. *ACS Earth Space Chem.* **2022**, *6*, 380−390.
(37) Ying, Q.; Li, J.; Kota, S. H. Significant contributions of isoprene to summertime secondary organic aerosol in eastern United States. *Environ. Sci. Technol.* **2015**, *49*, 7834−7842.
(38) Budisulistiorini, S. H.; Nenes, A.; Carlton, A. G.; Surratt, J. D.; McNeill, V. F.; Pye, H. O. Simulating aqueous-phase isoprene-epoxydiol (IEPOX) secondary organic aerosol production during the 2013 Southern Oxidant and Aerosol Study (SOAS). *Environ. Sci. Technol.* **2017**, *51*, 5026−5034.
(39) Eddingsaas, N. C.; VanderVelde, D. G.; Wennberg, P. O. Kinetics and products of the acid-catalyzed ring-opening of atmospherically relevant butyl epoxy alcohols. *J. Phys. Chem. A* **2010**, *114*, 8106−8113.
(40) Gaston, C. J.; Riedel, T. P.; Zhang, Z.; Gold, A.; Surratt, J. D.; Thornton, J. A. Reactive uptake of an isoprene-derived epoxydiol to submicron aerosol particles. *Environ. Sci. Technol.* **2014**, *48*, 11178−11186.
(41) Woo, J. L.; McNeill, V. F. simpleGAMMA v1. 0−a reduced model of secondary organic aerosol formation in the aqueous aerosol phase (aaSOA). *Geosci. Model Dev.* **2015**, *8*, 1821−1829.
(42) Zhang, Y.; Chen, Y.; Lambe, A. T.; Olson, N. E.; Lei, Z.; Craig, R. L.; Zhang, Z.; Gold, A.; Onasch, T. B.; Jayne, J. T.; et al. Effect of the aerosol-phase state on secondary organic aerosol formation from the reactive uptake of isoprene-derived epoxydiols (IEPOX). *Environ. Sci. Technol. Lett.* **2018**, *5*, 167−174.
(43) Riva, M.; Bell, D. M.; Hansen, A.-M. K.; Drozd, G. T.; Zhang, Z.; Gold, A.; Imre, D.; Surratt, J. D.; Glasius, M.; Zelenyuk, A. Effect of organic coatings, humidity and aerosol acidity on multiphase chemistry of isoprene epoxydiols. *Environ. Sci. Technol.* **2016**, *50*, 5580−5588.
(44) Rasool, Q. Z.; Shrivastava, M.; Octaviani, M.; Zhao, B.; Gaudet, B.; Liu, Y. Modeling Volatility-Based Aerosol Phase State Predictions in the Amazon Rainforest. *ACS Earth Space Chem.* **2021**, *5*, 2910−2924.


https://doi.org/10.1021/acsearthspacechem.2c00358
ACS Earth Space Chem. XXXX, XXX, XXX−XXX

(45) Octaviani, M.; Shrivastava, M.; Zaveri, R. A.; Zelenyuk, A.; Zhang, Y.; Rasool, Q. Z.; Bell, D. M.; Riva, M.; Glasius, M.; Surratt, J. D. Modeling the Size Distribution and Chemical Composition of Secondary Organic Aerosols during the Reactive Uptake of Isoprene-Derived Epoxydiols under Low-Humidity Condition. *ACS Earth Space Chem.* **2021**, *5*, 3247−3257.
(46) Zhang, Z.; Lin, Y.-H.; Zhang, H.; Surratt, J. D.; Ball, L. M.; Gold, A. Synthesis of isoprene atmospheric oxidation products: isomeric epoxydiols and the rearrangement products cis-and trans-3-methyl-3, 4-dihydroxytetrahydrofuran. *Atmos. Chem. Phys.* **2012**, *12*, 8529−8535.
(47) Zelenyuk, A.; Imre, D.; Wilson, J.; Zhang, Z.; Wang, J.; Mueller, K. Airborne single particle mass spectrometers (SPLAT II & miniSPLAT) and new software for data visualization and analysis in a geo-spatial context. *J. Am. Soc. Mass Spectrom.* **2015**, *26*, 257−270.
(48) Anttila, T.; Kiendler-Scharr, A.; Tillmann, R.; Mentel, T. F. On the reactive uptake of gaseous compounds by organic-coated aqueous aerosols: Theoretical analysis and application to the heterogeneous hydrolysis of N2O5. *J. Phys. Chem. A* **2006**, *110*, 10435−10443.
(49) Zaveri, R. A.; Easter, R. C.; Wexler, A. S. A new method for multicomponent activity coefficients of electrolytes in aqueous atmospheric aerosols. *J. Geophys. Res.: Atmos.* **2005**, *110*, No. D02201.
(50) Wexler, A. S.; Clegg, S. L. Atmospheric aerosol models for systems including the ions H+, NH4+, Na+, SO42−, NO3−, Cl−, Br−, and H2O. *J. Geophys. Res.: Atmos.* **2002**, *107*, ACH 14-11−ACH14-14.
(51) Nguyen, T. B.; Coggon, M. M.; Bates, K. H.; Zhang, X.; Schwantes, R. H.; Schilling, K. A.; Loza, C. L.; Flagan, R. C.; Wennberg, P. O.; Seinfeld, J. H. Organic aerosol formation from the reactive uptake of isoprene epoxydiols (IEPOX) onto non-acidified inorganic seeds. *Atmos. Chem. Phys.* **2014**, *14*, 3497−3510.
(52) Riedel, T. P.; Lin, Y.-H.; Zhang, Z.; Chu, K.; Thornton, J.; Vizuete, W.; Gold, A.; Surratt, J. Constraining condensed-phase formation kinetics of secondary organic aerosol components from isoprene epoxydiols. *Atmos. Chem. Phys.* **2016**, *16*, 1245−1254.
(53) Lin, Y.-H.; Zhang, Z.; Docherty, K. S.; Zhang, H.; Budisulistiorini, S. H.; Rubitschun, C. L.; Shaw, S. L.; Knipping, E. M.; Edgerton, E. S.; Kleindienst, T. E.; et al. Isoprene epoxydiols as precursors to secondary organic aerosol formation: acid-catalyzed reactive uptake studies with authentic compounds. *Environ. Sci. Technol.* **2012**, *46*, 250−258.
(54) Surratt, J. D.; Gómez-González, Y.; Chan, A. W.; Vermeylen, R.; Shahgholi, M.; Kleindienst, T. E.; Edney, E. O.; Offenberg, J. H.; Lewandowski, M.; Jaoui, M.; et al. Organosulfate formation in biogenic secondary organic aerosol. *J. Phys. Chem. A* **2008**, *112*, 8345−8378.
(55) Zaveri, R. A.; Easter, R. C.; Shilling, J. E.; Seinfeld, J. Modeling kinetic partitioning of secondary organic aerosol and size distribution dynamics: representing effects of volatility, phase state, and particle-phase reaction. *Atmos. Chem. Phys.* **2014**, *14*, 5153−5181.
(56) Zaveri, R. A.; Easter, R. C.; Fast, J. D.; Peters, L. K. Model for simulating aerosol interactions and chemistry (MOSAIC). *J. Geophys. Res.: Atmos.* **2008**, *113*, No. D13204.
(57) Roldin, P.; Eriksson, A.; Nordin, E.; Hermansson, E.; Mogensen, D.; Rusanen, A.; Boy, M.; Swietlicki, E.; Svenningsson, B.; Zelenyuk, A.; Pagels, J. Modelling non-equilibrium secondary organic aerosol formation and evaporation with the aerosol dynamics, gas-and particle-phase chemistry kinetic multilayer model ADCHAM. *Atmos. Chem. Phys.* **2014**, *14*, 7953−7993.
(58) Xing, L.; Shrivastava, M.; Fu, T.-M.; Roldin, P.; Qian, Y.; Xu, L.; Ng, N. L.; Shilling, J.; Zelenyuk, A.; Cappa, C. D. Parameterized Yields of Semivolatile Products from Isoprene Oxidation under Different NO X Levels: Impacts of Chemical Aging and Wall-Loss of Reactive Gases. *Environ. Sci. Technol.* **2018**, *52*, 9225−9234.
(59) He, Y.; King, B.; Pothier, M.; Lewane, L.; Akherati, A.; Mattila, J.; Farmer, D. K.; McCormick, R. L.; Thornton, M.; Pierce, J. R.; et al. Secondary organic aerosol formation from evaporated biofuels: comparison to gasoline and correction for vapor wall losses. *Environ. Sci.: Processes Impacts* **2020**, *22*, 1461−1474.
(60) Akherati, A.; He, Y.; Coggon, M. M.; Koss, A. R.; Hodshire, A. L.; Sekimoto, K.; Warneke, C.; De Gouw, J.; Yee, L.; Seinfeld, J. H.; et al. Oxygenated aromatic compounds are important precursors of secondary organic aerosol in biomass-burning emissions. *Environ. Sci. Technol.* **2020**, *54*, 8568−8579.
(61) Krechmer, J. E.; Pagonis, D.; Ziemann, P. J.; Jimenez, J. L. Quantification of gas-wall partitioning in Teflon environmental chambers using rapid bursts of low-volatility oxidized species generated in situ. *Environ. Sci. Technol.* **2016**, *50*, 5757−5765.
(62) He, Y.; Akherati, A.; Nah, T.; Ng, N. L.; Garofalo, L. A.; Farmer, D. K.; Shiraiwa, M.; Zaveri, R. A.; Cappa, C. D.; Pierce, J. R.; Jathar, S. H. Particle size distribution dynamics can help constrain the phase state of secondary organic aerosol. *Environ. Sci. Technol.* **2021**, *55*, 1466−1476.
(63) Matsunaga, A.; Ziemann, P. J. Gas-wall partitioning of organic compounds in a Teflon film chamber and potential effects on reaction product and aerosol yield measurements. *Aerosol Sci. Technol.* **2010**, *44*, 881−892.
(64) McMurry, P. H.; Grosjean, D. Photochemical formation of organic aerosols: growth laws and mechanisms. *Atmos. Environ. (1967)* **1985**, *19*, 1445−1451.
(65) Shrivastava, M.; Cappa, C. D.; Fan, J.; Goldstein, A. H.; Guenther, A. B.; Jimenez, J. L.; Kuang, C.; Laskin, A.; Martin, S. T.; Ng, N. L.; et al. Recent advances in understanding secondary organic aerosol: Implications for global climate forcing. *Rev. Geophys.* **2017**, *55*, 509−559.
(66) Riedel, T. P.; Lin, Y.-H.; Budisulistiorini, S. H.; Gaston, C. J.; Thornton, J. A.; Zhang, Z.; Vizuete, W.; Gold, A.; Surratt, J. D. Heterogeneous reactions of isoprene-derived epoxides: reaction probabilities and molar secondary organic aerosol yield estimates. *Environ. Sci. Technol. Lett.* **2015**, *2*, 38−42.
(67) Mozurkewich, M.; McMurry, P. H.; Gupta, A.; Calvert, J. G. Mass accommodation coefficient for HO2 radicals on aqueous particles. *J. Geophys. Res.: Atmos.* **1987**, *92*, 4163−4170.
(68) Frauenheim, M.; Offenberg, J.; Zhang, Z.; Surratt, J. D.; Gold, A. The C5−Alkene Triol Conundrum: Structural Characterization and Quantitation of Isoprene-Derived C5H10O3 Reactive Uptake Products. *Environ. Sci. Technol. Lett.* **2022**, *9*, 829.
(69) Zelenyuk, A.; Cai, Y.; Chieffo, L.; Imre, D. High precision density measurements of single particles: The density of metastable phases. *Aerosol Sci. Technol.* **2005**, *39*, 972−986.
(70) Surratt, J. D.; Lewandowski, M.; Offenberg, J. H.; Jaoui, M.; Kleindienst, T. E.; Edney, E. O.; Seinfeld, J. H. Effect of acidity on secondary organic aerosol formation from isoprene. *Environ. Sci. Technol.* **2007**, *41*, 5363−5369.
(71) Ye, Q.; Goss, M. B.; Krechmer, J. E.; Majluf, F.; Zaytsev, A.; Li, Y.; Roscioli, J. R.; Canagaratna, M.; Keutsch, F. N.; Heald, C. L.; Kroll, J. H. Product distribution, kinetics, and aerosol formation from the OH oxidation of dimethyl sulfide under different RO 2 regimes. *Atmos. Chem. Phys.* **2022**, *22*, 16003−16015.
(72) Bates, K. H.; Cope, J. D.; Nguyen, T. B. Gas-Phase Oxidation Rates and Products of 1, 2-Dihydroxy Isoprene. *Environ. Sci. Technol.* **2021**, *55*, 14294−14304.
(73) Porter, W. C.; Jimenez, J. L.; Barsanti, K. C. Quantifying atmospheric parameter ranges for ambient secondary organic aerosol formation. *ACS Earth Space Chem.* **2021**, *5*, 2380−2397.


https://doi.org/10.1021/acsearthspacechem.2c00358
*ACS Earth Space Chem.* XXXX, XXX, XXX−XXX